



Parametric Amplification at Ka Band via Nonlinear Dynamics in Superconducting 3D Cavities

D. Banys¹ · M. A. McCulloch¹ · S. Azzoni¹ · B. Cooper¹ · A. J. May^{1,2,3} · S. J. Melhuish¹ · L. Piccirillo^{1,4} · J. Wenninger¹

Received: 21 August 2019 / Accepted: 3 March 2020 / Published online: 18 March 2020
© The Author(s) 2020

Abstract

Modern parametric amplifiers are based on lithographically produced superconducting thin-film planar transmission line structures. These paramps rely on resonant structures with embedded nonlinear elements to stimulate intermodulation with a stronger pump tone that gives rise to signal gain when certain conditions are satisfied. Such paramps have not yet been realised in superconducting 3D waveguide resonators. Possible applications of these devices include detector systems that are based on 3D waveguide such as dark matter detectors and quantum computers. Reported here are the results of an investigation of a 30.64 GHz series circular waveguide resonance machined from bulk niobium showing parametric gain of up to 2 dB in the presence of a stronger pump tone 10 kHz above in frequency. The gain is largest on abrupt jumps of the transmission spectra of the resonance, which may be a result of weak-link formation on the superconducting surfaces.

Keywords Ka band · Parametric amplifier · Superconducting 3D cavity · Circular waveguide

1 Introduction

In the last decade, a re-emerging type of low-noise amplifier (LNA) has been extensively investigated in the microwave frequency domain, that is, the parametric amplifier. These paramps promise high wideband gain with high dynamic ranges

✉ D. Banys
danielius.banys@manchester.ac.uk

¹ Jodrell Bank Centre for Astrophysics, University of Manchester, Manchester M13 9PL, UK

² STFC Daresbury Laboratory, Keckwick Lane, Warrington WA4 4AD, UK

³ Cockcroft Institute, Keckwick Lane, Warrington WA4 4AD, UK

⁴ Engineering Research Institute Ventspils International Radio Astronomy Centre (ERI VIRAC), University of Applied Sciences (VUAS), Inzenieru Street 101, Ventspils LV-3601, Latvia

and quantum-limited noise performance. Most modern paramps make use of superconducting transmission lines (STLs) such as co-planar waveguides (CPWs) or microstrips with embedded nonlinear elements to enable parametric gain. Commonly, Josephson junctions (JJs) [1, 2] or weak links [3, 4] which exhibit an inductance that is nonlinear with current are exploited. However, due to their low critical currents, these extrinsic nonlinear elements greatly limit the dynamic range of the amplifier which makes these devices inappropriate for many high power or multiplexing applications. The dynamical range can be increased by several orders of magnitude by instead exploiting the intrinsic nonlinear kinetic inductance (KI) of STLs [5], which is greatly enhanced in thin superconducting (SC) films. The early modern paramps made use of a resonant cavity [1, 3, 4] to provide high gain with noise levels that were below that of vacuum fluctuations when noise squeezing [6] techniques were employed, but the gain of these paramps was limited to occur within the bandwidth of the resonance of the cavity. More recent paramps solved the bandwidth issue by using electrically long transmission lines with embedded JJs [2] or by exploiting the nonlinear KI of SC thin films [5].

In this paper, we show that it is possible to achieve parametric gain with a 3D STL. In our case, a circular waveguide (WG) cavity is used to provide a sufficient nonlinearity for parametric processes to take place. Compared to lithographically produced paramps, 3D WG paramps could offer benefits in the form of simplified fabrication methods, physical durability, use of true WG thermal breaks [7] and simpler scalability to frequencies of up to a few hundred GHz and be integrated with systems that use 3D WG in their structure via low-loss transitions. If high gain, frequency tunability of the resonance frequency and near quantum-limited noise performance can be achieved while also isolating the pump tone from the application in question, such 3D WG paramps could be applied directly as the readout of axion detectors such as MADMAX [8] or as readout amplifiers for qubits generated in a 3D circuit quantum electrodynamics (cQED) architectures [9].

Reported in this work are the results from an investigation of a cryogenically cooled bulk niobium circular WG cavity with resonances within the Ka (26.5–40 GHz) band. The measurements show a 2 dB signal gain with input power of -60 dBm in the presence of a stronger pump tone when both tones are positioned 10 kHz apart within a 30.64 GHz resonance. This parametric gain occurs predominantly on the lower side of the resonance along abrupt jumps of the transmission spectrum. Interestingly, the opposite side of the resonance exhibits parametric signal attenuation of a similar order to the gain. Possible explanations of this gain spectrum may come in the form of phase-mismatch arguments between the signal, pump and generated idler tones. The source of the abrupt jumps in transmission is also explored.

2 Parametric Amplification in 3D Waveguide

A nonlinearity of a STL can be used for mixing of propagating waves and the generation of new tones. Under certain conditions, this intermodulation can result in parametric signal gain. One such STL nonlinearity is the intrinsic KI nonlinearity, which can be

derived from BCS theory [10]. This KI allows for the modulation of the reactive component of the surface impedance of a transmission line and gives rise to the necessary parametric processes. The KI in a thin SC strip at temperatures $T \ll T_c$ takes the form of Eq. 1 when expanded to the first quadratic term [11],

$$L_k(I) = L_k(0) \left(1 + \frac{I^2}{I_*^2} + \dots \right), \quad (1)$$

where $L_k(0)$ is the KI per unit length in the low power and linear limit, I_* is the characteristic current which sets the scale of the quadratic nonlinearity and I is the current applied to the transmission line. A nonlinear inductance can also arise due to a supercurrent flow through a weak contact between two superconductors; these structures are called weak links and can be described by the Josephson effect [12]. Their critical currents depend on the type of link that exists between the two superconducting parts. In general, the inductance of a weak link or JJ [13] takes the form of

$$L_j(I) = \frac{\hbar}{2eI_c} \frac{\arcsin(I/I_c)}{I/I_c}, \quad (2)$$

where I_c is the critical current and I is the current flowing through the junction or weak link, respectively. In 3D STLs, such as circular waveguide, the supercurrent flows along the walls of the structure. The current distributions are dependent on the chosen mode of propagation. The nonlinearities that exist in these waveguides depend on factors such as the choice of SC material, machining techniques and surface treatments.

Parametric amplification exploits the outlined nonlinearities of the system and can take place via a process called degenerate four-wave mixing (FWM). This can be explained by considering two incident tones at the input of a nonlinear transmission line, that is, a weak signal at frequency ω_s and a strong pump at frequency ω_p . As the two tones co-propagate in the transmission line, the nonlinearity of the line causes a new tone to be produced at the beat frequency of the two waves, $\omega_p - \omega_s$. This beat tone then modulates the surface impedance of the superconductor and produces sidebands around each incident tone at frequencies $\omega_p \pm (\omega_p - \omega_s)$ and $\omega_s \pm (\omega_p - \omega_s)$. The amplitude of these sidebands is proportional to the amplitude of the respective phase-modulated tone. Most of the generated components are much weaker than either input tone, except for the sideband at $\omega_i = 2\omega_p - \omega_s$, which is referred to as the idler. This idler also participates in the mixing process and causes additional side bands to be produced. Some of the generated sidebands in both of these processes overlap with the signal, causing its amplitude to increase; this is referred to as parametric gain [14, 15].

To control the direction of energy flow between the involved propagating waves, it is important to consider the phase mismatch between the tones as well as the coupled mode equations of each propagating wave [5, 14]. The low-power propagation mismatch between the four involved waves is

$$\Delta\beta = 2\beta(\omega_p) - \beta(\omega_s) - \beta(\omega_i), \quad (3)$$

where $\beta(\omega_{p,s,i})$ are the propagation constants of the pump, signal and idler, respectively. In a dispersionless medium, $\Delta\beta = 0$ constitutes perfect phase matching and is the condition for maximum parametric gain. Using Eq. 3, the overall phase mismatch between the four involved waves can be determined using

$$\theta(z) = \Delta\beta z + 2\phi_p(z) - \phi_s(z) - \phi_i(z), \quad (4)$$

where $\phi_{p,s,i}$ are the phases of each propagating wave at some distance z along the transmission line. These phases include the initial phase at $z = 0$ and the phase acquired due to any nonlinear phase shift. By controlling the phase relation in Eq. 4, it is possible to control the direction of the flow of energy, that is, from the pump to the signal and idler ($\theta(z) = \pi/2$) or from the signal and idler to the pump ($\theta(z) = -\pi/2$). These results can be derived from the general coupled mode equations of co-propagating waves in a transmission medium with a Kerr nonlinearity [14].

In reality, dispersion due to material or waveguide properties can affect the phase slippage between the involved waves as they propagate, which in turn can change whether the signal is amplified or deamplified. This dispersion can be mitigated by introducing anomalous dispersion into the propagating structure, which allows for a phase matching condition to be attained for some small signal bandwidth. One such method is to use a resonance that is engineered into the transmission line which introduces modified dispersion properties near the resonance frequency.

Since rectangular or circular waveguides are indeed dispersive, a constant phase relationship between tones at large frequency separation cannot remain true without introducing anomalous dispersion into the structure. In the case of a series resonator, if the incident signal and pump remain close in frequency and within the bandwidth of the resonance, the waveguide dispersion differences can be kept to a minimum. Hence, fine-tuning of the effective dispersion that each tone experiences may be possible in order to attain phase matching.

3 Cavity Fabrication and Measurement Setup

Circular WG cavities were fabricated by milling out bulk niobium rod. The associated covers that included a coupling aperture were fabricated from the same rod and were attached to the resonator body through mounting holes of a standard Ka band rectangular WG flange—shown in Fig. 1. The irises act as impedance boundaries and allow for standing waves to form between the two terminations. Two variants of the circular WG cavities were fabricated, the first with one port exhibited a much larger loaded quality factor, Q_L , since this is the sum of the inverse of the internal quality factor of the cavity, Q_i , and the coupling apertures, Q_c , i.e. $Q_L^{-1} = Q_i^{-1} + Q_c^{-1}$. This single input cavity could be used in a combination with a circulator to extract useful parametric gain. A second cavity with two ports allowed for transmission measurements, which was the focus of this work. The internal and coupling quality factors can be determined from fitting to a resonance curve. The cavities were

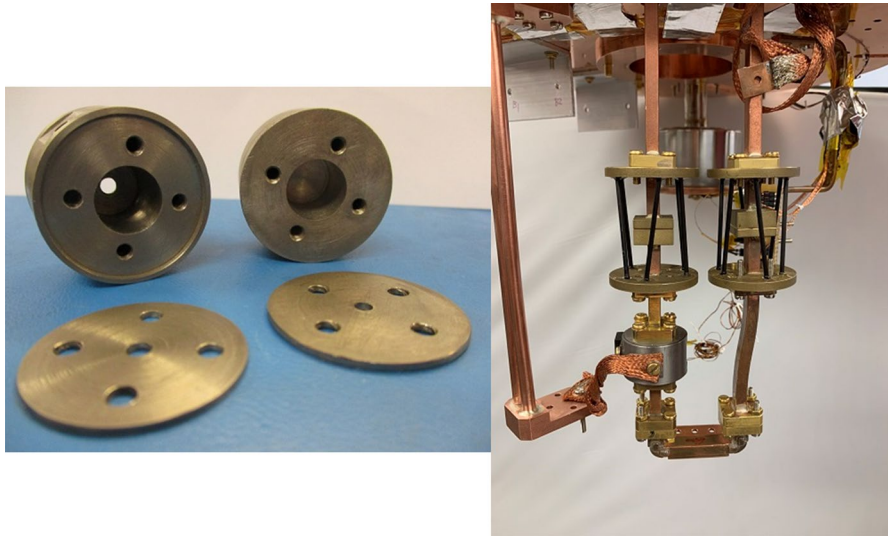


Fig. 1 Left: Circular WG cavities of inner diameter 11.9 mm and length 15.7 mm made from annealed niobium rod (99.9% purity). The cavities had multiple covers with circular apertures that were different in diameter and thickness in order to investigate different coupling regimes. After machining, the cavities were cleaned in sonicated chemical baths consisting of Decon 90 detergent, acetone and isopropyl alcohol. Right: The transmission cavity mounted inside the test cryostat and thermally connected to the 2.6 K stage of the cryostat via a copper strap. The cavity can be connected to the 1 K cold head of the sorption cooler (behind thermal breaks) via a copper bracket that is not shown in the figure (Color figure online)

simulated extensively in ANSYS HFSS¹—a 3D finite element method Maxwell equation solver—where the modes of the circular WG cavity resonances could be individually excited and identified.

Prior to cryogenic testing, the cavities were chemically cleaned and then baked in an oven at 200 °C to remove any remaining water on the surface. Following this treatment, the cavities were mounted inside a cryogen-free cryostat based around a SHI Cryogenics² RDK-415D cold head, providing a nominal cold-stage temperature of 2.6 K. Heaters mounted to the cold stage were used to raise the temperature of this stage as required. In order to provide the capacity to operate the resonator at $1\text{ K} < T < 2.6\text{ K}$, a helium ⁴He adsorption cooler was installed. (Operation and performance of this cooler are described in detail in Refs. [16–18].) The resonators were thermally isolated by multiple stages of Ka band WG thermal breaks [7]; the full WG chain had a total attenuation of around 2 dB when the SC cavities were replaced by a WG through. A photograph of the last stage of thermal isolation is shown in Fig. 1. Outside the cryostat, the signal and pump tones were generated internally by two separate sources within a vector network analyser, as shown in

¹ www.ansys.com/.

² www.shicryogenics.com/.

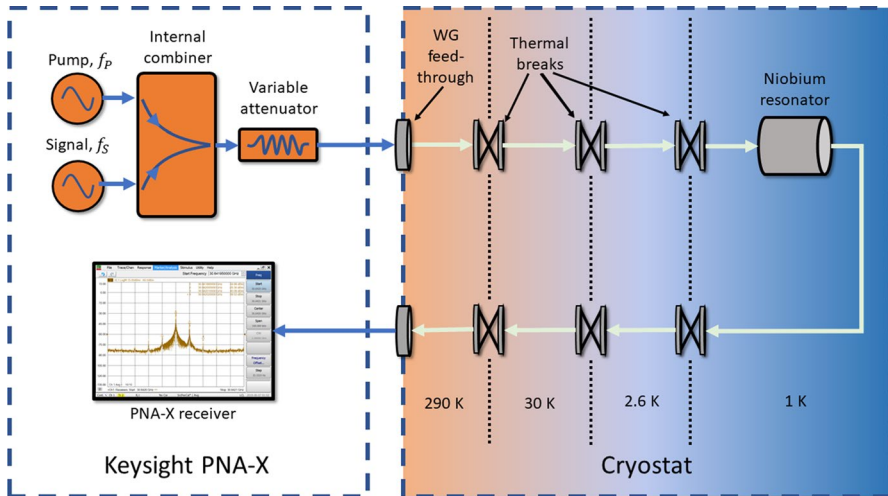


Fig. 2 Schematic view of the signal flow from the generation of the two tones by separate sources within a Keysight N5245A PNA-X, through to the cryostat via Ka band copper rectangular waveguide and into the internal receiver of the PNA-X. Due to the limitation of both tones being attenuated by a single attenuator bank, the maximum power difference between the tones was 30 dB. The IF bandwidth of the PNA-X was kept at 100 Hz for the measurements (Color figure online)

Fig. 2, where they were internally combined and passed through a single attenuator bank.

4 Analysis and Results

The tested two-port circular waveguide cavity had a number of resonances within the Ka band. A TM_{110} resonance at 30.64 GHz was chosen due to it having the largest loaded quality factor of 5×10^3 and the highest transmission value. Initially, single-tone transmission measurement was taken at a range of input powers corresponding to the sum of the signal and pump powers that were used in the subsequent two-tone tests. This provided a direct comparison of the single-tone transmission spectra with the values that were traced out by the continuous-wave (CW) pump tone during the two-tone test. This single-tone transmission data in Fig. 3 shows that there is a change in coupling with increasing input power, which can be attributed to surface impedance change. There does not seem to be a shift down in resonance frequency with input power, nor a bending of the resonance shape which would be visible if a large nonlinear KI was present and the oscillator was approaching its bifurcation regime [19, 20]. This is an indicator that the KI fraction relative to the total inductance in this resonator geometry is very small. This is expected since the KI fraction is proportional to the magnetic field surface area integral relative to that of the volume [21]. However, above -45 dBm in pump power, a series of jumps appear in the transmission spectra; up to four jumps are observed for a given input power. The true nature of these jumps is not

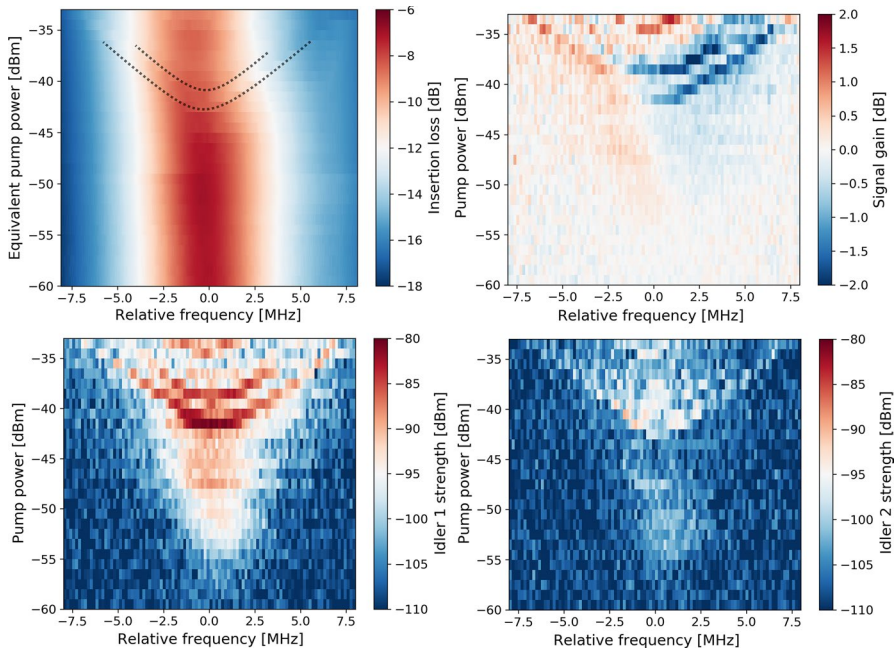


Fig. 3 Investigation of a SC circular waveguide cavity TM_{110} resonance. The plots are centred at the resonance frequency of 30.64 GHz. Top left: Single-tone transmission at various input powers. Equivalent pump power (total power – signal power) is used for a more direct visual comparison with the gain data. Two dotted lines are included to draw attention to the positions of discontinuities in transmission. The waveguide feedline losses were not calibrated out. Top right: The gain in signal power relative to the transmission spectrum that is traced out by the pump tone. The signal was kept at a constant -60 dBm and 10 kHz below the pump tone as the two tones were swept through the profile of the resonance. Bottom left: The power of the idler at $f_{i,1} = 2f_p - f_s$. The receiver noise floor was at -110 dBm. Bottom right: The power of the idler at $f_{i,2} = 2f_s - f_p$ (Color figure online)

known, but it is hypothesised that these could be weak-link features that were also observed by Abdo et al. [22] in stripline resonators. The weak links were thought to be a result of impurities causing normal-state hot spots to form in the path of the supercurrent. This effect may also be occurring in the SC circular waveguides due to distributed impurities in the relatively dirty (99.9% purity) niobium rod that was used in the manufacture of these resonators. However, this requires further investigation of the RF properties of these jumps, as well as characterisation of the surface properties of the resonator walls.

It should be noted that no magnetic shielding was used around the cavities. This may have allowed external fields to interact with the weak-link features or create vortex pinning sites that added additional RF losses to the resonator. Shifts in the resonance shape and position were observed when all other system parameters were kept constant. This had the effect of adding noise to the S-parameter measurements of the cavities and possibly obscuring any small shifts in resonance frequency due to nonlinear inductances. A magnetic shield is currently

being developed to significantly attenuate any external magnetic field that may be interacting with the resonator.

For the two-tone measurements, the VNA was set up such that the output of each source was a single-frequency CW signal. The sources of the VNA were power calibrated at the input of the cryostat and the receiver was calibrated with one of the VNA sources. During the test, the pump was kept above the signal in frequency at a constant spacing, and the tones were swept together over the profile of the resonance. To evaluate if any signal gain has occurred, the received power of the signal was referenced to a transmission spectrum that was traced out by the pump tone. Since the received signal power was measured simultaneously to that of the pump, using the inferred pump transmission rather than the single-tone transmission as the reference point helped to avoid the effect of a changing resonance shape, which occurred due to the lack of magnetic shielding. Using the pump transmission as a reference relied on the assumption that the pump tone did not become depleted as a result of the parametric processes that have taken place. This assumption is likely to breakdown as the pump power approaches the -60 dBm input power of the signal.

The signal gain and the generated idler strengths are shown in Fig. 3. The gain data show that the signal experiences an increase in transmission of up to 2 dB positioned mostly on the jumps that are observed in the single-tone transmission data. Above the resonance frequency, there are regions where the signal experiences parametric attenuation on the same jumps in transmission. These regions of signal gain/attenuation correspond with regions where the idlers at $f_{i,1} = 2f_p - f_s$ and $f_{i,2} = 2f_s - f_p$ are also strongly generated, which adds further evidence of FWM occurring. A possible explanation for this signal gain shape is currently under investigation. A preliminary analysis, which will be presented in future publications, of the phase across the resonance and the arguments made using Eq. 4 is suggesting that the weak-link features with steeper anomalous dispersion are creating opposite phase-mismatch conditions on one side of the resonance relative to the other. The phase mismatch is different by as much as π radians, which is enough to reverse the power flow from the pump to signal and idler to the opposite. An investigation of different frequency spacing between the involved tones may vary this phase mismatch in a more controlled manner and provide greater insight into this problem.

5 Conclusion

It was demonstrated that parametric amplification is possible not only in lithographically produced SC planar thin-film devices but also in bulk niobium circular waveguide cavities fabricated by simple milling techniques. An investigation of the insertion loss across a TM_{110} resonance at 30.64 GHz with changing input power did not show a shift in resonance frequency that would be characteristic of a strong nonlinear kinetic inductance. This may suggest that the quality factor is too low for this effect to be seen or that the kinetic inductance fraction is very weak for such a structure. This claim needs to be confirmed by investigating cavities with much larger quality factors and/or larger surface areas relative to their volume. In addition, a series of abrupt jumps in the transmission spectrum appeared for tone powers

above -45 dBm. These are similar to the jumps observed in [22] and may be due to a nonlinearity that is similar to that of weak links, which form as a result of distributed impurities in a SC transmission lines.

The introduction of a CW pump tone in the presence of -60 dBm CW signal yielded signal gain relative to transmission of up to 2 dB. This gain was positioned on sudden jumps in the transmission spectrum. Interestingly, the signal experienced parametric attenuation of a similar magnitude on the opposite side of the resonance to where the signal gain occurred. A possible explanation for this gain/attenuation may lie in the phase-mismatch condition of Eq. 4 that may be satisfied for opposing parametric processes by the steeper anomalous dispersion close to the weak-link features. However, a more detailed investigation of the phase and dispersion of a signal over the resonance is required.

Applications of such 3D WG paramps in the fields of dark matter detection and quantum computing were outlined. In order to be useful for these applications, important milestones need to be reached for these devices, that is, the observed signal gain should be much higher (at least above 10 dB) to be beneficial as a front-end amplifier; the gain curve should be tunable; and the noise performance should be quantum-limited. The next series of devices is being fabricated; these are based on split-block rectangular waveguide. The split-block arrangement allows for more complex resonator shapes to be machined. In addition to being made from bulk niobium, these cavities will also be made from copper and coated in series of films including a thin film of NbTiN. The coated cavities will have a much higher quality factor due to the much smoother cavity surface, and a larger London penetration depth which may enhance the kinetic inductance and improve the possible gain. A surface characterisation of the deposited films may also provide insight for the source of the weak-link features that appear in the transmission spectra of the cavities. Methods for frequency tunability of the resonance and therefore the gain curve are also being investigated.

Acknowledgements D. Banys was supported by a STFC PhD studentship.

Open Access This article is licensed under a Creative Commons Attribution 4.0 International License, which permits use, sharing, adaptation, distribution and reproduction in any medium or format, as long as you give appropriate credit to the original author(s) and the source, provide a link to the Creative Commons licence, and indicate if changes were made. The images or other third party material in this article are included in the article's Creative Commons licence, unless indicated otherwise in a credit line to the material. If material is not included in the article's Creative Commons licence and your intended use is not permitted by statutory regulation or exceeds the permitted use, you will need to obtain permission directly from the copyright holder. To view a copy of this licence, visit <http://creativecommons.org/licenses/by/4.0/>.

References

1. M.A. Castellanos-Beltran, K.D. Irwin, G.C. Hilton, L.R. Vale, K.W. Lehnert, *Nat. Phys.* **4**, 929 (2008)
2. C. Macklin, K. O'Brien, D. Hover, M.E. Schwartz, V. Bolkhovskoy, X. Zhang, W.D. Oliver, I. Siddiqi, *Science* **350**, 307 (2015)

3. E.A. Tholen, A. Ergul, E.M. Doherty, F.M. Weber, F. Grégis, D.B. Haviland, Appl. Phys. Lett. **90**, 253509 (2007). <https://doi.org/10.1063/1.2750520>
4. B. Abdo, E. Segev, O. Shtempluck, E. Buks, Appl. Phys. Lett. **88**, 022508 (2006). <https://doi.org/10.1063/1.2164925>
5. B.H. Eom, P.K. Day, H.G. LeDuc, J. Zmuidzinas, Nat. Phys. **8**, 623 (2012)
6. A.A. Clerk, M.H. Devoret, S.M. Girvin, F. Marquardt, R.J. Schoelkopf, Rev. Mod. Phys. **82**, 1155 (2010)
7. S.J. Melhuish, M.A. McCulloch, L. Piccirillo, C. Stott, Rev. Sci. Instrum. **87**, 104706 (2016). <https://doi.org/10.1063/1.4964475>
8. A. Caldwell, G. Dvali, B. Majorovits, A. Millar, G. Raffelt, J. Redondo, O. Reimann, F. Simon, F. Steffen, (MADMAX Working Group), Phys. Rev. Lett. **118**, 091801 (2017)
9. S. Kundu, N. Gheeraert, S. Hazra, T. Roy, K.V. Salunkhe, M.P. Patankar, R. Vijay, Appl. Phys. Lett. **114**, 172601 (2019). <https://doi.org/10.1063/1.5089729>
10. R. Parmenter, RCA (Radio Corporation of America) Review (U.S.), <https://www.osti.gov/biblio/5086098-nonlinear-electrodynamics-superconductors-very-small-coherence-distance>
11. J. Zmuidzinas, Annu. Rev. Condens. Matter Phys. **3**, 169 (2012). <https://doi.org/10.1146/annurev-conmatphys-020911-125022>
12. K.K. Likharev, Rev. Mod. Phys. **51**, 101 (1979)
13. M.A. Castellanos-Beltran, K.W. Lehnert, Appl. Phys. Lett. **91**, 083509 (2007). <https://doi.org/10.1063/1.2773988>
14. J. Hansryd, P.A. Andrekson, M. Westlund, J. Li, P.O. Hedekvist, IEEE J. Sel. Top. Quantum Electron. **8**, 506 (2002)
15. A.S. Kher, *Superconducting Nonlinear Kinetic Inductance Devices*, Ph.D. thesis, California Institute of Technology, Pasadena, California, 2017
16. A.J. May, *Sub-Kelvin Cryogenics for Experimental Cosmology*, Ph.D. thesis, University of Manchester, Manchester, 2019
17. A.J. May, G. Coppi, V. Haynes, S. Melhuish, L. Piccirillo, T. Sarmento, S. Teale, Cryogenics **102**, 45 (2019)
18. L. Piccirillo, G. Coppi, A. May, *Miniature Sorption Coolers: Theory and Applications* (CRC Press, Boca Raton, 2018)
19. B. Yurke, E. Buks, J. Lightwave Technol. **24**, 5054 (2006)
20. L.J. Swenson, P.K. Day, B.H. Eom, H.G. Leduc, N. Llombart, C.M. McKenney, O. Noroozian, J. Zmuidzinas, J. Appl. Phys. **113**, 104501 (2013). <https://doi.org/10.1063/1.4794808>
21. E.T. Holland, Y.J. Rosen, N. Materise, N. Woollett, T. Voisin, Y.M. Wang, S.G. Torres, J. Mireles, G. Carosi, J.L. DuBois, Appl. Phys. Lett. **111**, 202602 (2017). <https://doi.org/10.1063/1.5000241>
22. B. Abdo, E. Segev, O. Shtempluck, E. Buks, Phys. Rev. B **73**, 134513 (2006)

Publisher's Note Springer Nature remains neutral with regard to jurisdictional claims in published maps and institutional affiliations.